# Bonding Nature of Open-Lantern-type Dinuclear Cr(II) Complexes. Theoretical Study with the MRMP2 Method

**Yusaku I. Kurokawa, Yoshihide Nakao, and Shigeyoshi Sakaki***

*Department of Molecular Engineering, Graduate School of Engineering, Kyoto University, Nishikyo-ku, Kyoto 615-8510, Japan*

*Received: October 30, 2008; Revised Manuscript Received: January 27, 2009*

Open-lantern-type dinuclear Cr(II) complex, $[Cr(R^1NC(R^2)NR^3)_2]_2$ ($R^1$ = Et, $R^2$ = Me, and $R^3$ = $^t$Bu), was theoretically investigated with DFT, CASSCF, and MRMP2 methods. The DFT-optimized Cr−Cr distance (1.757 Å) is too short compared to the experimental value (1.960 Å). The CASSCF method does not present the minimum in the range of the Cr−Cr distance from 1.75 to 2.05 Å. The MRMP2 method presents the optimized Cr−Cr distance of 1.851 Å, which is a little shorter than the experimental value. These results suggest that both nondynamical and dynamical correlations are considerably large in this complex. The Cr−Cr bond order is evaluated to be 2.40 with the CASSCF method, which is much smaller than the formal bond order of 4. In the Mo analogue, on the other hand, the DFT, CASSCF, and MRMP2 methods present almost the same Mo−Mo distance (2.151 Å). The Mo−Mo bond order is evaluated to be 3.41, which is somewhat smaller than the formal value but much larger than the Cr−Cr bond order. These differences arise from the much larger d−d overlap integral of the Mo−Mo pair than that of the Cr−Cr pair. Though nondynamical correlation effect is very large in this dinuclear Cr(II) complex, the Cr−Cr distance of this complex was experimentally discussed to be short, based on formal shortness ratio (FSR). We wish to propose here orbital shortness ratio (OSR) based on the distance providing maximum overlap integral to discuss the M−M bond distance. According to the OSR, we understand that the Cr−Cr distance of 1.960 Å is long but the Mo−Mo distance of 2.151 Å is short. This understanding is consistent with much larger nondynamical correlation in the dinuclear Cr(II) complex than in the Mo(II) analogue. Interesting differences are also observed between M−M and Si−Si multiple bonds. The differences are discussed in terms of $\sigma$- and $\pi$-type overlap integrals and the participation of Si 3s orbital in the $\sigma$-bonding orbital.

## 1. Introduction

The metal−metal multiple bond is one of the interesting and challenging research targets in inorganic, physical, and theoretical chemistries. For instance, the Re−Re quadruple bond was very previously proposed by Cotton and his collaborators,[1,2] but correct understanding of its bonding nature has been recently achieved by theoretical works with CASPT2 and MRMP2 methods.[3,4] Another good example is dinuclear Cr compounds including the Cr−Cr multiple bond. Cr dimer, $Cr_2$, is of considerable interest because it is believed to possess a hextuple Cr−Cr bond in a formal sense, which is the largest bond order at this moment.[5] Theoretical calculation of this compound is challenging because of the presence of very large electron correlation effects. Actually, a lot of theoretical work has been carried out with sophisticated methods including CASPT2, MR-CI, and similar methods.[6] Also, RCrCrR (R = $C_6H_3$-2,6 ($C_6H_3$-2,6-$Pr^i_2$)$_2$), which was recently synthesized by Power and his collaborators,[7] has drawn a lot of interest because it possesses a Cr−Cr quintuple bond and its trans-bent geometry is similar to that of $E_2R_2$ molecule bearing E−E triple bond (E = Si to Pb; R = bulky aryl or silyl ligand). Theoretical studies of this compound have been carried out with DFT[8,9] and CASPT2 methods.[10] Though the Cr−Cr bond order was calculated to be 4.64 with the DFT method, it was 3.52 by the CASSCF calculation, indicating that the nondynamical correlation effects are considerably large in this complex.[9] Recently, lantern-type Cr(I) dinuclear complex was experimentally reported.[11] Interestingly, its Cr−Cr distance is very short.

**SCHEME 1: (A) Lantern-type Complex and (B) Open-Lantern-type Complex**[a]

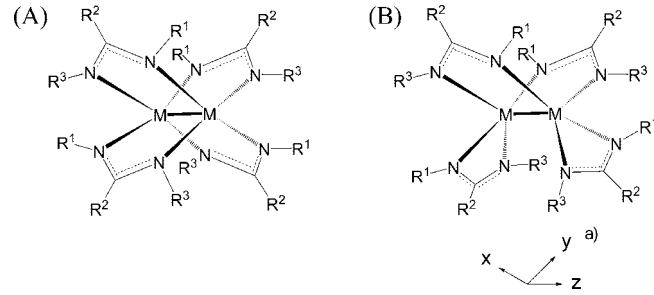


[a] The *z*-axis is along the M−M bond, and the *x*- and *y*-axes are along M−N bonds.

Besides these dinuclear Cr(I) complexes, experimental and theoretical studies on dinuclear Cr(II) complexes bearing Cr−Cr quadruple bond have been reported previously.[12−28] Though most of them take lantern-type structure (Scheme 1A), open lantern-type dinuclear Cr(II) complex was recently reported (Scheme 1B).[28] This complex possesses a short Cr−Cr bond (1.9601 Å) like $[Li(L)]_4[Cr_2Me_8]$ (Cr−Cr = 1.98 Å, L = THF or $Et_2O$) and [(tetraazaannulene)$Cr_2$] (Cr−Cr = 2.096 Å). Interestingly, this complex easily dissociates to two mononuclear Cr(I) complexes in solution unlike $[Li(L)]_4[Cr_2Me_8]$ (L = THF or $Et_2O$) in spite of its short Cr−Cr bond, even when Lewis

* Corresponding author. E-mail: sakaki@moleng.kyoto-u.ac.jp.

10.1021/jp809597m CCC: $40.75 
Published on Web 03/09/2009

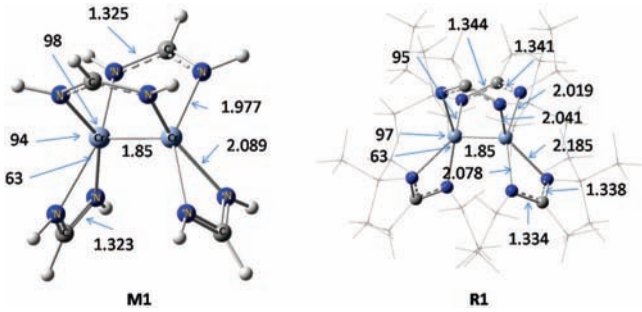


**Figure 1.** DFT-optimized geometries of $[Cr(R^1NC(R^2)NR^3)_2]_2$ ($R^1$ = $R^2$ = $R^3$ = H) (**M1**) and $[Cr(R^1NC(R^2)NR^3)_2]_2$ ($R^1$ = Et, $R^2$ = Me, and $R^3$ = $^t$Bu) (**R1**) at $R$(Cr−Cr) = 1.85 Å. **M1** and **R1** take $C_{2v}$ and $C_2$ symmetries, respectively. In **R1**, the high-level region of the ONIOM calculation is drawn with balls and sticks, and the low-level region is drawn with wire frame. Length in angstroms and angle in degrees.

base is not added. Though there remain these interesting issues to be investigated, theoretical study of the open-lantern-type dinuclear Cr(II) complex has not been carried out yet, to our best knowledge.

In this theoretical study, we investigated open-lantern-type dinuclear Cr(II) complex, $[Cr(R^1NC(R^2)NR^3)_2]_2$ ($R^1$ = Et, $R^2$ = Me, and $R^3$ = $^t$Bu) (**R1**), with DFT, CASSCF, and MRMP2 methods. Our purposes here are to clarify the Cr(II)−Cr(II) bonding nature and to characterize the Cr(II)−Cr(II) quadruple bond by making comparison with the Mo(II)−Mo(II) quadruple bond, and to present clear comparison between the Cr(II)−Cr(II) quadruple and Si−Si multiple bonds.

## 2. Models and Computational Details

Because the real complex, $[Cr(R^1NC(R^2)NR^3)_2]_2$ ($R^1$ = Et, $R^2$ = Me, and $R^3$ = $^t$Bu) (**R1**), is very large, we employed a small model (**M1**) in preliminary calculations. In **M1**, all alkyl substituents were replaced with hydrogen atoms, as shown in Figure 1.

Their geometries were optimized at various Cr−Cr distances in singlet spin state, where the DFT method was employed with B3LYP functional.[29] Potential energy surface (PES) was calculated with the MRMP2 method,[4] where the CASSCF wave function was taken as the reference. In the CASSCF calculation, eight electrons in the eight orbitals $\sigma_d$, $\pi 1_d$, $\pi 2_d$, $\delta_d$, $\sigma_d$*, $\pi 1_d$*, $\pi 2_d$*, and $\delta_d$* were taken as active space because these orbitals exist around the HOMO and LUMO, as shown in Scheme 2. This calculation is named CASSCF(8,8) hereafter. The $d_{x^2-y^2}$ orbital was excluded from the active space because it exists at much higher energy due to the strong antibonding interaction with the lone pair orbitals of ligands; see Scheme 1 for the coordinate. This active space is the same as those of CASPT2 and MRMP2 calculations of dinuclear Re complex, $[Re_2Cl_8]^{2-}$, bearing a Re−Re quadruple bond.[30,31]

The total energy of the real system, $E_{real}$, was evaluated by the ONIOM method.[32] The ONIOM-calculated energy is represented as

$$E_{real} = E_{real,\ low} - E_{model,\ low} + E_{model,\ high} \quad (1)$$

where $E_{real,\ low}$ and $E_{model,\ low}$ are the energies of the real and model systems calculated at low level of theory, respectively, and $E_{model,\ high}$ is that of the model system calculated at high level of theory. These energy values were calculated separately and assembled according to eq 1. We applied the DFT method to the whole system and either the CASSCF or MRMP2 method to the high-quality region throughout the present study. They are named ONIOM(CASSCF:DFT) and ONIOM(MRMP2:DFT), respectively, hereafter.

**SCHEME 2: Active Orbitals Employed in the CASSCF(8,8) Calculation**[a]

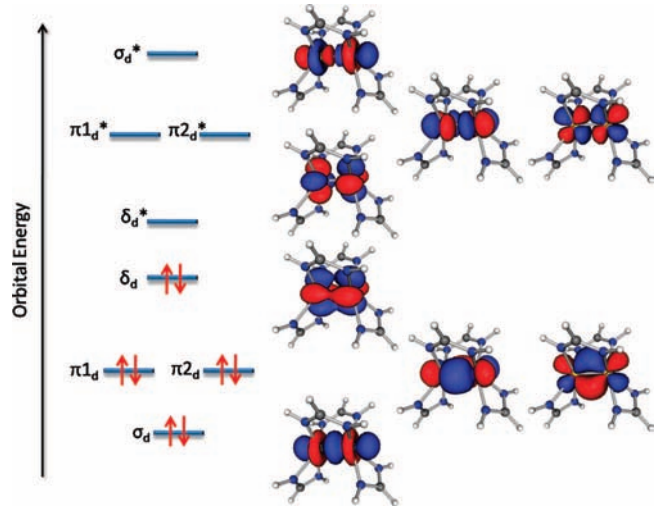


[a] Arrows represent Hartree−Fock configuration.

Core electrons (up to 2p) of Cr were replaced with Stuttgart−Dresden−Born effective core potentials (ECPs), and its valence electrons were represented with a (311111/22111/411/1) basis set.[33] This basis set is named SDD hereafter. For C, N, and H, cc-pVDZ basis sets were employed. The s-, p-, and d-type augmented functions were added to N because it is anionic in the ligand. The SDD basis set was employed for Mo, too.

To clarify the characteristic features of the Cr−Cr quadruple bond, we compared it with the Si−Si triple bond of $Si_2H_2$ molecule (**S1**) and Si−Si double bond of $Si_2H_4$ molecule (**S2**). The geometries of **S1** and **S2** were optimized in $C_{2h}$ symmetry by the DFT method with B3LYP functional, where cc-pVTZ basis sets were employed for Si and cc-pVDZ basis set for H. The optimized geometries are shown in Figure S1. Also, we carried out the CASSCF(6,6) calculation of **S1** and the CASSCF(4,4) calculation of **S2** using the DFT-optimized geometry. In the CASSCF(6,6) calculation of **S1**, six electrons in the six orbitals $\sigma_p$, $\pi 1_p$, $\pi 2_p$, $\sigma_p$*, $\pi 1_p$*, and $\pi 2_p$* were taken as an active space, as shown in Scheme 3. In the CASSCF(4,4) calculation of **S2**, four electrons in the four orbitals $\sigma_p$, $\pi_p$, $\sigma_p$*, and $\pi_p$* were taken as an active space. We ascertained that the shapes of Kohn−Sham orbitals of **S1** are similar to those of real compounds, 1,1,4,4-tetrakis[bis(trimethslsilyl)methyl]-1,4-diisopropyl-2-tetrasilyne;[34] see Supporting Information Figure S2.

Gaussian 03[35] and GAMESS[36] program packages were used for DFT, CASSCF, and MRMP2 calculations, respectively. Molecular orbitals (MOs) were drawn with the Molekel program.[37]

## 3. Results and Discussion

**3.1. Preliminary Examination of Model Compound $[Cr(R^1NC(R^2)NR^3)_2]_2$ ($R^1$ = $R^2$ = $R^3$ = H) (M1).** We optimized the structure of **M1** at various Cr−Cr distances under $C_{2v}$ symmetry, as shown in Figure 1. Very small imaginary frequency with $B_2$ symmetry does not disappear in the optimized geometry,[38] probably because the Cr−Cr distance is fixed. In the DFT-optimized geometry, the Cr−Cr distance is 1.757 Å, as shown in Figure 2, which is much shorter than the

**SCHEME 3: Active Orbitals Employed in the CASSCF(6,6) Calculation of HSi≡SiH (S1) (A) and the CASSCF(4,4) Calculation of $H_2Si{=}SiH_2$ (S2) (B)[a]**

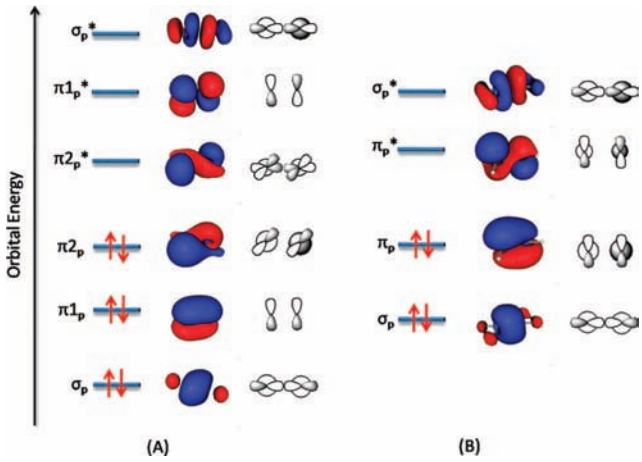


[a] Arrows represent Hartree−Fock configuration.

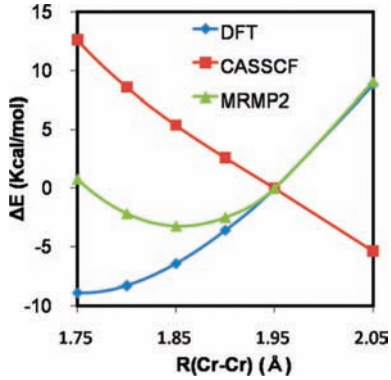


**Figure 2.** PESs of $[Cr(R^1NC(R^2)NR^3)_2]_2$ ($R^1 = R^2 = R^3 = H$) (**M1**) calculated by the DFT, CASSCF, and MRMP2 methods. The energy of $R$(Cr−Cr) = 1.95 Å is taken to be standard (energy zero); $E_{DFT}$ = −771.824 45 au, $E_{CASSCF}$ = −766.901 80 au, and $E_{MRMP2}$ = −769.851 97 au at this distance.

**TABLE 1: Occupation Numbers of the Natural Orbitals and the Bond Order of $[Cr(R^1NC(R^2)NR^3)_2]_2$ ($R^1 = R^2 = R^3$ = H) (M1), $[Cr(R^1NC(R^2)NR^3)_2]_2$ ($R^1$ = Et, $R^2 = CH_3$, and $R^3$ = $^t$Bu) (R1), and $[Mo(R^1NC(R^2)NR^3)_2]_2$ ($R^1 = R^2 = R^3$ = H) (Mo1)[a]**

| | M1 | R1 | Mo1 |
|---|---|---|---|
| $R$(M−M) (Å) | 1.85 | 1.85 | 2.15 |
| $\sigma_d$ | 1.740 | 1.723 | 1.895 |
| $\pi 1_d$ | 1.707 | 1.693 | 1.88 |
| $\pi 2_d$ | 1.713 | 1.683 | 1.884 |
| $\delta_d$ | 1.372 | 1.299 | 1.753 |
| $\delta_d$* | 0.629 | 0.702 | 0.247 |
| $\pi 2_d$* | 0.294 | 0.318 | 0.117 |
| $\pi 1_d$* | 0.287 | 0.308 | 0.12 |
| $\sigma_d$* | 0.259 | 0.276 | 0.104 |
| bond order | | | |
| $\sigma_d$ | 0.741 | 0.724 | 0.896 |
| $\pi_d$ | 1.420 | 1.375 | 1.764 |
| $\delta_d$ | 0.372 | 0.299 | 0.753 |
| total | 2.532 | 2.397 | 3.412 |

[a] The CASSCF(8,8) method was employed.

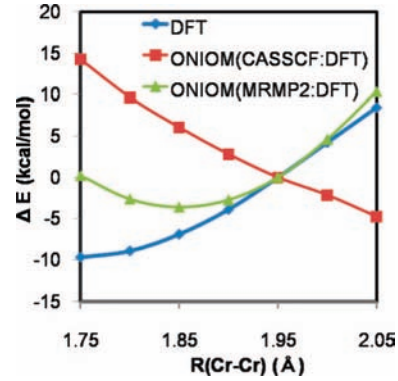


**Figure 3.** PESs of $[Cr(R^1NC(R^2)NR^3)_2]_2$ ($R^1$ = Et, $R^2$ = Me, and $R^3$ = $^t$Bu) (**R1**) calculated by the DFT, ONIOM(CASSCF:DFT), and ONIOM(MRMP2:DFT) methods. The energy of $R$(Cr−Cr) = 1.95 Å is taken to be standard (energy zero); $E_{DFT}$ = −1872.520 05 au, $E_{ONIOM(CASSCF:DFT)}$ = −1867.606 36 au, and $E_{ONIOM(MRMP2:DFT)}$ = −1870.552 63 au at this distance.

experimental value by 0.2 Å. One can expect that geometry optimization of **M1** in nonet spin state yields longer Cr−Cr distance. However, the minimum energy was not observed in the range of $R$(Cr−Cr) = 1.85−3.6 Å, and the nonet spin state is more than 100 kcal/mol above the singlet spin state at $R$(Cr−Cr) = 1.85 Å; see Supporting Information Figure S4.

Also, we carried out the CASSCF(8,8) calculation of **M1**, using the DFT-optimized geometry. The PES smoothly decreases as the Cr−Cr distance increases unlike the DFT-calculated PES, as shown in Figure 2. However, the equilibrium structure is not presented in the range of $R$(Cr−Cr) = 1.75−2.15 Å. Completely different PES between CASSCF and DFT calculations suggests the presence of very large nondynamical correlation effect.

In MRMP2 calculations, the Cr−Cr distance is optimized to be 1.855 Å (Figure 2), which is moderately longer than that of the DFT-optimized distance by 0.1 Å but moderately shorter than that of the experimental value by 0.1 Å.[28] These results suggest that both nondynamical and dynamical correlations play important roles to present correctly the Cr−Cr distance of **M1**.

The occupation number of each natural orbital was calculated with the CASSCF(8,8) method, as shown in Table 1. The difference in the occupation number between $\delta_d$ and $\delta_d$* orbitals is 0.743, which is much smaller than 2. This is the main source of the large nondynamical correlation. The bond order is defined as one-half of the difference between the sum of occupation numbers in the bonding orbitals and that of the antibonding orbitals. In **M1**, the bond order is evaluated to be 2.53 at $R$(Cr−Cr) = 1.850 Å. This value is much smaller than the formal bond order (4.0) of the quadruple bond. This very small bond order arises from the occupations of antibonding orbitals, $\sigma_d$*, $\pi 1_d$*, $\pi 2_d$*, and $\delta_d$* orbitals, which will be discussed below in more detail.

**3.2. Geometry and Bonding Nature of Real Complex, $[Cr(R^1NC(R^2)NR^3)_2]_2$ ($R^1$ = Et, $R^2$ = Me, and $R^3$ = $^t$Bu) (R1).** The geometry of **R1** was optimized by the DFT method at various Cr−Cr distances. The optimized geometry at each Cr−Cr distance takes $C_2$ symmetry in which no imaginary frequency is observed. The DFT-calculated PES decreases as the Cr−Cr distance becomes shorter, but the equilibrium structure is not found in the range $R$(Cr−Cr) > 1.75 Å, as shown in Figure 3. In contrast to the DFT-calculated PES, the ONIOM(CASSCF:DFT)-calculated PES decreases as the Cr−Cr distance becomes longer. The equilibrium structure is not found, too, in the range of $R$(Cr−Cr) < 2.05 Å. On the other hand, the ONIOM(MRMP2:DFT)-calculated PES exhibits the minimum at $R$(Cr−Cr) = 1.851 Å. These features of the PESs are essentially the same as those of **M1**.

The Cr−Cr bond order is evaluated to be 2.40 with the CASSCF(8,8) method at $R$(Cr−Cr) = 1.850 Å. This value is

**TABLE 2: Important Electron Configurations and Their Coefficients for $[Cr(R^1NC(R^2)NR^3)_2]_2$ ($R^1$ = Et, $R^2$ = Me, and $R^3$ = $^t$Bu) (R1) and $[Mo(R^1NC(R^2)NR^3)_2]_2$ ($R^1 = R^2 = R^3$ = H) (Mo1)[a]**

| R1 | | Mo1 | |
|---|---|---|---|
| coefficients | configuration | coefficients | configuration |
| 0.632 75 | $\sigma_d^2\pi 1_d^2\pi 2_d^2\delta_d^2$ | 0.867 16 | $\sigma_d^2\pi 1_d^2\pi 2_d^2\delta_d^2$ |
| −0.394 94 | $\sigma_d^2\pi 1_d^2\pi 2_d^2\delta_d^{*2}$ | −0.259 24 | $\sigma_d^2\pi 1_d^2\pi 2_d^2\delta_d^{*2}$ |
| −0.154 46 | $\sigma_d^2\pi 1_d^2\delta_d^2\sigma_d^{*2}$ | −0.117 54 | $\sigma_d^2\pi 1_d^2\delta_d^2\pi 1_d^{*2}$ |
| 0.113 81 | $\sigma_d^2\pi 1_d^2\delta_d^{*2}\sigma_d^{*2}$ | −0.103 46 | $\sigma_d^2\pi 1_d^2\pi 2_d^2\pi 1_d^{*2}$ |
| −0.196 69 | $\sigma_d^2\pi 1_d^2\pi 2_d^2\delta_d^1\delta_d^{*1}\sigma_d^{*1}$ | −0.112 21 | $\sigma_d^2\pi 2_d^2\delta_d^2\pi 2_d^{*2}$ |
| −0.153 84 | $\sigma_d^2\pi 1_d^2\pi 2_d^2\delta_d^1\delta_d^{*1}\pi 1_d^{*1}$ | −0.137 37 | $\sigma_d^2\pi 1_d^2\pi 2_d^2\delta_d^1\delta_d^{*1}\pi 1_d^{*1}$ |
| −0.130 33 | $\sigma_d^2\pi 1_d^1\pi 2_d^2\delta_d^1\delta_d^{*1}\pi 2_d^{*1}$ | −0.133 60 | $\sigma_d^1\pi 1_d^2\pi 2_d^2\delta_d^1\delta_d^{*1}\sigma_d^{*1}$ |
| −0.124 91 | $\sigma_d^1\pi 1_d^2\pi 2_d^2\delta_d^1\delta_d^{*1}\pi 2_d^{*1}$ | 0.107 62 | $\sigma_d^2\pi 1_d^1\pi 2_d^2\delta_d^1\delta_d^{*1}\pi 2_d^{*1}$ |
| 0.121 02 | $\sigma_d^1\pi 1_d^2\pi 2_d^2\delta_d^1\delta_d^{*1}\pi 1_d^{*1}$ | | |
| −0.104 68 | $\sigma_d^2\pi 1_d^1\pi 2_d^1\delta_d^2\pi 2_d^{*1}\sigma_d^{*1}$ | | |
| −0.101 86 | $\sigma_d^2\pi 1_d^1\pi 2_d^1\delta_d^2\pi 2_d^{*1}\pi 1_d^{*1}$ | | |

[a] The CASSCF(8,8) method was employed.

moderately smaller than that of **M1**, as shown in Table 1. It is noted that the $\pi_d$ and $\delta_d$ bond orders are considerably smaller in **R1** than in **M1** by 0.045 and 0.073, respectively, though the $\sigma_d$ bond order is slightly smaller in **R1** than in **M1** by 0.017. The smaller $\pi_d$ and $\delta_d$ bond orders arise from the fact that **M1** takes $C_{2v}$ symmetry but **R1** takes $C_2$ symmetry. The $d_\pi$ and $d_\delta$ atomic orbitals of one Cr atom overlap worse with those of the other Cr atom in the $C_2$ symmetry than in the $C_{2v}$ symmetry, because the $d_\pi$ and $d_\delta$ atomic orbitals of one Cr atom twist with respect to those of the other Cr atom in the $C_2$ symmetry. Thus, their bonding interactions become weaker in **R1**. However, the $\sigma_d$ bond order is not different very much between **M1** and **R1** because the $d_\sigma$ atomic orbital of one Cr atom overlaps well with that of the other Cr atom in both $C_2$ and $C_{2v}$ symmetries; note that the twist distortion little changes the direction of $d_\sigma$ atomic orbital.

The CASSCF(8,8) wave function of the high-quality region of **R1**, $\Psi_{\mathbf{R1},\,CAS(8,8)}$, is represented as follows

$$\Psi_{\mathbf{R1},CAS(8,8)} = 0.633\Phi_{main} - 0.395\Phi_{\delta^2\rightarrow\delta^{*2}} - 0.197\Phi_{\pi 2^2\delta^2\rightarrow\pi 2\delta\delta^*\sigma^*} - 0.154\Phi_{\pi 2^2\rightarrow\sigma^{*2}} - 0.154\Phi_{\pi 1^2\delta^2\rightarrow\pi 1\delta\delta^*\pi 1^*} + \cdots \quad (2)$$

where $\delta$, $\delta^*$, etc. represent $\delta_d$, $\delta_d^*$, etc. (see Scheme 2), respectively, here. The main configuration is $\sigma_d^2\pi 1_d^2\pi 2_d^2\delta_d^2$, which is the same as the Hartree−Fock configuration. However, its expansion coefficient is only 0.633, and its weight is 40.1%. The second leading configuration is $\sigma_d^2\pi 1_d^2\pi 2_d^2\delta_d^{*2}$, the weight of which is very large, being over one-third of that of the main configuration. This configuration corresponds to excitation of two electrons from $d_\delta$ to $d_\delta^*$, as expected. The expansion coefficient of the third leading configuration, $\sigma_d^2\pi 1_d^2\pi 2_d^1\delta_d^1\delta_d^{*1}\sigma_d^{*1}$, is unexpectedly large, 0.197, too. Also, it is noted that not $\pi_d^*$ orbital but $\sigma_d^*$ orbital participates in the third and fourth excited configurations (see Table 2). This is against our expectation that the $\delta_d \rightarrow \pi_d^*$ excited configuration is energetically lower than the $\delta_d \rightarrow \sigma_d^*$ excited configuration because the $\sigma_d^*$ is in general at higher energy than the $\pi_d^*$. This unexpected result will be discussed below in detail. The other configurations with large expansion coefficients are listed in Table 2. Apparently, the wave function of **R1** consists of many electron configurations including various kinds of excitations. This result clearly indicates that the nondynamical electron correlation is very large.

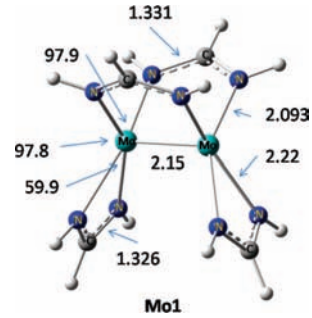


**Figure 4.** DFT-optimized geometry of $[Mo(R^1NC(R^2)NR^3)_2]_2$ ($R^1 = R^2 = R^3$ = H) (**Mo1**) at $R$(Mo−Mo) = 2.15 Å. Length in angstroms and angle in degrees.

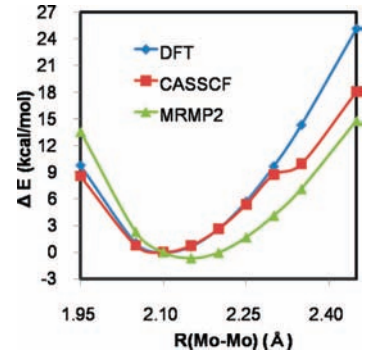


**Figure 5.** PESs of $[Mo(R^1NC(R^2)NR^3)_2]_2$ ($R^1 = R^2 = R^3$ = H) (**M2**) calculated by the DFT, CASSCF, and MRMP2 methods. The energy of $R$(Mo−Mo) = 2.10Å is taken to be standard (energy zero); $E_{DFT}$ = −734.398 94 au, $E_{CASSCF}$ = −729.469 70 au, and $E_{MRMP2}$ = −732.531 51 au at this distance.

We wish to mention here the possibility that the third and fourth leading configurations involve one-electron excitation due to mixing of metal $d_\delta$, $d_\pi$, and $d_\sigma$ orbitals because of the low symmetry ($C_2$) of **R1** and that it is not the case anymore for the open-lantern complexes.[21b] To check this possibility, we carried out CASSCF(8,8) calculation of closed-lantern-type dinuclear Cr(II) complex taking $D_{2h}$ symmetry (Scheme 1A). This calculation indicates that similar one-electron excited configuration is involved in the third leading term in the CASSCF(8,8) wave function. Thus, one-electron excited configuration is not a result of low symmetry of open-lantern-type structure: see Supporting Information pages S-18−S-21 for details.

**3.3. Geometry and Electronic Structure of the Molybdenum Analogue, $[Mo(R^1NC(R^2)NR^3)_2]_2$ ($R^1 = R^2 = R^3$ = H) (Mo1).** Though the Mo analogue of **R1** has not been synthesized yet, we investigated the Mo analogue of **M1**, $[Mo(R^1NC(R^2)NR^3)_2]_2$ ($R^1 = R^2 = R^3$ = H) (**Mo1**), to shed clear light on characteristic features of the dinuclear Cr(II) complex by making comparison between **M1** and **Mo1**. We optimized the geometry of **Mo1** with the DFT(B3LYP) method under $C_{2v}$ symmetry, as shown in Figure 4. No imaginary frequency was observed at each optimized geometry. The DFT-calculated energy minimum is found at $R$(Mo−Mo) = 2.106 Å, as shown in Figure 5. CASSCF(8,8) and MRMP2 calculations present the energy minimum at $R$(Mo−Mo) = 2.101 and 2.151 Å, respectively. It is noted that all these methods present almost the same equilibrium Mo−Mo distance. This result is completely different from that of the dinuclear Cr(II) complex, indicating that very large difference in electronic structure exists between dinuclear Cr(II) and Mo(II) complexes.

The occupation numbers of important natural orbitals calculated by the CASSCF(8,8) method are shown in Table 1.

Apparently, the occupation numbers of bonding orbitals are considerably larger than those of antibonding orbitals. The bond order at $R$(Mo−Mo) = 2.150 Å is evaluated to be 3.41, which is much larger than that of **M1**; see Table 1. The $\sigma_d$ bond order is close to 1.0. The $\pi_d$ and $\delta_d$ bond orders are 1.764 and 0.572, respectively, which are much larger than those of **M1**. From these results, it should be concluded that all the $\sigma_d$, $\pi_d$, and $\delta_d$-bonding interactions are much stronger in **Mo1** than in **M1**.

The CASSCF(8,8) wave function of **Mo1**, $\Psi_{\mathbf{Mo1},\,\mathrm{CAS(8,8)}}$, is represented as follows

$$\Psi_{\mathbf{Mo1},\mathrm{CAS(8,8)}} = 0.867\Phi_{\mathrm{main}} - 0.259\Phi_{\delta^2\rightarrow\delta^{*2}} - 0.137\Phi_{\pi 2^2\delta^2\rightarrow\pi 2\delta\delta^*\pi 1^*} - 0.133\Phi_{\pi 1^2\delta^2\rightarrow\pi 1\delta\delta^*\pi 2^*} - 0.118\Phi_{\pi 2^2\rightarrow\pi 2^{*2}} + \cdots \quad (3)$$

The main configuration is $\sigma_d^2\pi 1_d^2\pi 2_d^2\ \delta_d^2$. Though this is the same as that of **M1**, its expansion coefficient is much larger than that of **M1**. The second leading configuration is $\sigma_d^2\pi 1_d^2\pi 2_d^2\delta_d^{*2}$. Though this configuration is the same as that of **M1**, its expansion coefficient is much smaller than that of **M1**. The other configurations with large expansion coefficients are listed in Table 2. Apparently, the numbers of electron configurations are less in **Mo1** than in **M1**. All these results clearly show that the nondynamical correlation is much smaller in **Mo1** than in **M1**, as expected above.

**3.4. The Reason Why Nondynamical Correlation Is Much Larger in the Dinuclear Cr(II) Complex than in the Dinuclear Mo(II) Complex.** In many cases, the Cr−Cr distance was discussed on the basis of the Cotton's formal shortness ratio (FSR).[12b] The FSR for an A−B bond is defined by eq 4

$$\mathrm{FSR_{AB}} = \frac{R_{\mathrm{A-B}}}{R_{\mathrm{A}} + R_{\mathrm{B}}} \quad (4)$$

where $R_{A-B}$ is the A−B bond length in a molecule and $R_A$ and $R_B$ are the atomic radii of A and B, respectively. Many dinuclear Cr complexes have been reported to exhibit FSR value either similar to or smaller than that of dinitrogen molecule ($FSR_{N-N}$ = 0.783);[12b] for instance, $FSR_{Cr-Cr}$ for **R1** is 0.780 at $R$(Cr−Cr) = 1.850 Å and 0.826 at $R$(Cr−Cr) = 1.96 Å which is the experimental value. These results suggest that the Cr−Cr bond of **R1** is similar to the very strong N−N triple bond. Actually, the M−M bond shorter than 2.0 Å is found in many dinuclear Cr and several dinuclear V complexes[12b,39,40] but not at all in the other transition metal complexes.[12b] Based on these facts, the Cr−Cr distance of 1.96 Å was discussed to be "short".[12b] However, the nondynamical correlation is very large in the dinuclear Cr(II) complex. This is against our expectation that the nondynamical correlation tends to be small when the bond distance is short. This unexpected result suggests that the FSR is not useful to discuss the Cr−Cr distance of this complex. Actually, it is likely that the FSR calculated with the atomic radius of neutral Cr(0) leads to an unusually small FSR value because the atomic radius of Cr(0) is determined by the 4s orbital but the valence orbital of Cr(II) is 3d; note that the Cr(0) 4s orbital is much larger than the Cr(II) 3d orbital.

Because the bond distance depends on the orbital expansion, the bond distance must be discussed on the basis of orbital overlap. Here, we evaluated the mean radii, $\langle r\rangle$, of the radial distribution function of valence orbital and the distance, $R_{Smax}$, providing the maximum overlap integral. It is likely that the bond distance directly depends on the $2 \times \langle r\rangle$ and $R_{Smax}$ values.

**TABLE 3: $\langle r\rangle$[a] and $R_{Smax}$[b] Values of Valence Orbitals of Si, Cr, and Mo**

| | Si 3p[c] | Cr 3d[c] | Mo 4d[d] |
|---|---|---|---|
| $\langle r\rangle$ (Å) | 1.4719 | 0.7333 | 0.9785 |
| $2 \times \langle r\rangle$ (Å) | 2.9438 | 1.4666 | 1.9571 |
| $R_{Smax}$ (Å) | | | |
| $\sigma-\sigma$ | 2.4529 | 1.5200 | 2.5144 |
| $\pi-\pi$ | − | 1.1473 | 1.4697 |

[a] Mean value of radial distribution function. [b] The distance between two atoms which provides the maximum overlap integral. [c] Calculated with ANO basis proposed by Roos et al.[42] [d] Calculated with Huzinaga's basis.[43]

**TABLE 4: d−d and p−p Overlap Integrals[a] of Cr−Cr, Mo−Mo, and Si−Si Pairs**

| | M = Cr[a] ($R$ = 1.85 Å) | M = Mo[b] ($R$ = 2.15 Å) | M = Si[a] ($R$ = 2.10 Å) |
|---|---|---|---|
| $d_\sigma-d_\sigma$ (or $p_\sigma-p_\sigma$) | 0.0764 | 0.1061 | 0.3143 |
| $d_\pi-d_\pi$ (or $p_\pi-p_\pi$) | 0.1295 | 0.2036 | 0.3282 |
| $d_\delta-d_\delta$ | 0.0672 | 0.0692 | − |

[a] Calculated with ANO basis proposed by Roos et al.[42] [b] Calculated with Huzinaga's basis.[43]

In Cr atom, $2 \times \langle r_{3d}\rangle$, $R_{Smax}^{3d_\sigma}$, and $R_{Smax}^{3d_\pi}$ values are calculated to be 1.466, 1.520, and 1.147 Å, respectively,[42] as shown in Table 3 and Figure S11. The Cr−Cr distance (1.960 Å) of this open-lantern-type dinuclear complex[28] is much longer than these values. On the other hand, the Mo−Mo distance (2.15 Å) of **Mo1** is moderately longer than $2 \times \langle r_{4d}\rangle$ and $R_{Smax}^{4d_\pi}$ values but much shorter than $R_{Smax}^{4d_\sigma}$ value, as shown in Table 3. These results indicate that the Cr−Cr quadruple bond of 1.960 Å is "long" but the Mo−Mo quadruple bond of 2.151 Å is either "medium" or "short". This understanding is consistent with the fact that the nondynamical correlation is very large in the dinuclear Cr(II) complex but moderate in the Mo analogue.

From the above results, it should be concluded that the $2 \times \langle r\rangle$ and $R_{Smax}$ values of valence d orbital must be employed to discuss whether the M−M bond is short or long. We wish to propose orbital shortness ratio (OSR) to discuss the M−M bond distance, as follows

$$\mathrm{OSR} = \frac{R_{\mathrm{M-M}}}{R_{S\mathrm{max}}^{\sigma}} \quad (5)$$

where $R_{Smax}^{\sigma}$ is employed because the $\sigma$-bonding interaction is always more important than the $\pi$-bonding interaction and also the $\pi$-bonding interaction is not always involved in dinuclear complexes. The OSR value is 1.217 for this open-lantern-type dinuclear Cr(II) complex and 0.854 for the Mo(II) analogue, indicating that the Cr−Cr distance should be understood to be long but the Mo−Mo distance is to be short. This OSR value also shows that the N−N distance of dinitrogen molecule is short; $OSR_{N-N}$ = 0.752. Note that this OSR value is similar to the FSR value in dinitrogen molecule.

The long separation between two Cr atoms leads to small overlap integral. Actually, the overlap integral for the Cr−Cr pair is much smaller than that for the Mo−Mo pair: the overlap integral is calculated to be 0.0764, 0.130, and 0.0672 for $d_\sigma-d_\sigma$, $d_\pi-d_\pi$, and $d_\delta-d_\delta$ pairs, respectively, at $R$ = 1.85 Å in the Cr complex and 0.106, 0.204, and 0.0692 at $R$ = 2.15 Å in the Mo complex, as shown in Table 4.

It should be noted that the Cr−Cr distance providing the maximum overlap integral of the $d_\sigma$ orbital is very short (1.52

**SCHEME 4: Electron Accumulation Regions in $d_\pi-d_\pi$ Bonding Orbital ($\pi_d$) and $d_\sigma-d_\sigma$ Bonding Orbital ($\sigma_d$)**

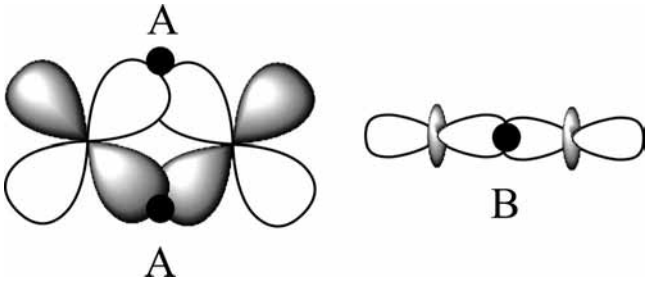


Å) but the Mo−Mo distance is long (2.51 Å). The overlap integral of $d_\sigma$ orbital is 0.0810 for the Cr−Cr pair at $R = 1.52$ Å and 0.117 for the Mo−Mo pair at $R = 2.51$ Å. These results clearly show that the d orbital of Cr is intrinsically much smaller than that of Mo, as was discussed previouly.[45] It is very difficult for the Cr−Cr pair to approach each other at the Cr−Cr distance of 1.52 Å; note that this distance is similar to the C−C single bond. Therefore, the Cr−Cr bond must stay at much longer distance than the $R^{3d_\sigma}_{Smax}$ value, leading to the much smaller overlap integral in the Cr−Cr pair than in the Mo−Mo pair. As a result, the nondynamical correlation is much larger in the dinuclear Cr(II) complex than in the dinuclear Mo(II) complex.

**3.5. Comparison between $d_\sigma-d_\sigma$ and $d_\pi-d_\pi$ Molecular Orbitals.** It should be noted that the $d_\sigma-d_\sigma$ overlap integral is much smaller than the $d_\pi-d_\pi$ overlap integral in both Cr−Cr and Mo−Mo pairs, as presented in Table 4. This is against our expectation that the overlap integral of the $\sigma$-type orbital is much larger than that of the $\pi$-type orbital. This unexpected result has not been reported yet, to our knowledge. However, this is not surprising because the $d_\pi-d_\pi$ overlap presents two overlap regions, as shown in Scheme 4. Despite the much larger overlap integral of the $d_\pi-d_\pi$ pair, the occupation numbers of the $\pi 1_d$ and $\pi 2_d$ natural orbitals are moderately smaller than that of the $\sigma_d$ orbital in both Cr and Mo dinuclear complexes, as shown in Table 1. It is worth investigating the reason why the occupation number of the $\sigma_d$ orbital is moderately larger than those of the $\pi 1_d$ and $\pi 2_d$ orbitals in spite of the much smaller $d_\sigma-d_\sigma$ overlap than the $d_\pi-d_\pi$ overlap in **R1** and **M1**.[41]

The $d_\pi$ atomic orbital expands perpendicular to the Cr−Cr axis, as shown in Scheme 4. Because the C−N bonds of the ligand exist near the $d_\pi-d_\pi$ overlap region, the exchange repulsion is induced between the $\pi 1_d$ and $\pi 2_d$ orbitals and doubly occupied orbitals of the C−N bonds, to push up the $\pi 1_d$ and $\pi 2_d$ orbital energies, which further leads to decrease of the occupation numbers of these orbitals. On the other hand, the $\sigma_d$ orbital expands along the Cr−Cr axis and little suffers from such exchange repulsion (Scheme 4). Thus, the occupation number of the $\sigma_d$ orbital becomes larger, but those of the $\pi 1_d$ and $\pi 2_d$ orbitals become smaller than those expected from overlap integral.

Another reason is that the $\pi 1_d$ and $\pi 2_d$ orbitals induce larger electrostatic repulsion with the negatively charged N atoms than does the $\sigma_d$ orbital. This is because the $\pi 1_d$ and $\pi 2_d$ orbitals are closer to the N atoms than the $\sigma_d$ orbital. As a result, the $\pi 1_d$ and $\pi 2_d$ orbital energies become higher and their occupation numbers become smaller than those expected from the overlap integral. This Coulombic repulsion also leads to the participation of the $\sigma_d$* orbital in the third and fourth leading terms of the CASSCF wave function. Because the $\pi 1_d$* and $\pi 2_d$* orbitals are also more destabilized by the Coulombic repulsion with the negatively charged N atom than the $\sigma_d$* orbital, electron occupations of the $\pi 1_d$* and $\pi 2_d$* orbitals lead to larger destabilization energy but that of the $\sigma_d$* orbital leads to smaller destabilization energy than those expected from overlap integral. This is one of the reasons why not the $\pi 1_d$* orbital but the $\sigma_d$* orbital participates in the third and fourth excited configurations of **R1**; see eq 1 and above discussion.

Also, the nuclear−electron Coulombic attraction participates in the larger occupation number of the $\sigma_d$ orbital than expected from overlap integral, as follows: electron accumulation mainly occurs around the region A in the $\pi 1_d$ and $\pi 2_d$ orbitals and the region B in the $\sigma_d$ orbital; see Scheme 4 for regions A and B. Because the region B is closer to the Cr atoms than the region A, the electron density in the region B yields larger nuclear−electron stabilization energy than that in the region A. Thus, the occupation number of the $\sigma_d$ orbital becomes larger, and those of the $\pi 1_d$ and $\pi 2_d$ orbitals become smaller than expected from the overlap integral.

All these are plausible factors for the smaller occupation numbers of the $\pi 1_d$ and $\pi 2_d$ orbitals and the larger one of the $\sigma_d$ orbital than expected from the overlap integral.

**TABLE 5: Occupation Numbers of the Natural Orbitals and the Bond Orders of S1 ($Si_2H_2$) and S2 ($Si_2H_4$)**

| | S1[a] | S2[b] |
|---|---|---|
| $\pi_p$ | 1.981 | 1.980 |
| $\pi 1_p$[c] | 1.880 | 1.867 |
| $\pi 2_p$[d] | 1.794 | − |
| $\pi 2_p$*[d] | 0.202 | − |
| $\pi 1_p$*[c] | 0.124 | 0.133 |
| $\sigma_p$* | 0.020 | 0.021 |
| bond order | | |
| $\sigma_p$ | 0.981 | 0.980 |
| $\pi_p$ | 1.674 | 0.867 |
| total | 2.655 | 1.847 |

[a] The CASSCF(6,6) method was employed. [b] The CASSCF(4,4) method was employed. [c] Out-of plane $\pi$ orbital. [d] In-plane $\pi$ orbital.

**3.6. Comparison between M−M and Si−Si Multiple Bonds.** Comparison of the multiple bonds between transition metal and nontransition metal compounds is expected to present clear insight into their bonding natures. We investigated here $Si_2H_2$, (**S1**), and $Si_2H_4$, (**S2**). The $\sigma_p$ and $\pi_p$ bond orders of **S1** were evaluated with the CASSCF method to be 0.981 and 1.674 (0.837 per one $\pi_p$ orbital, on average), respectively, and those of **S2** were evaluated to be 0.980 and 0.857, as shown in Table 5. It is noted that the occupation number of the $\sigma_p$ orbital is considerably larger than that of the $\pi_p$ orbital. This feature is different from that of the Cr−Cr and Mo−Mo multiple bonds.

In Si atom, $2 \times \langle r_{3p} \rangle$, $R^{3p_\sigma}_{Smax}$, and $R^{3p_\pi}_{Smax}$ values were calculated to be 2.944, 2.318, and 2.453 Å, respectively, as shown in Table 3 and Figure S10. In the usual Si−Si double and triple bonds, the Si−Si distance is 2.0 −2.3 Å,[44] which is much shorter than $2 \times \langle r_{3p} \rangle$, $R^{3p_\sigma}_{Smax}$, and $R^{3p_\pi}_{Smax}$ values. As a result, the OSR is small; the OSR value is 0.938 and 0.815 for the Si−Si double and triple bonds, respectively. Thus, the usual Si−Si double and triple bonds are defined to be short, which leads to large overlap integral between two Si atoms. Actually, the overlap integrals of the $p_\sigma-p_\sigma$ and $p_\pi-p_\pi$ orbital pairs in the Si−Si multiple bond are much larger than those of $d_\sigma-d_\sigma$ and $d_\pi-d_\pi$ orbital pairs in the M−M multiple bond, as shown in Table 4. Thus, the nondynamical correlation is small in **S1** and **S2**, as clearly shown by the considerably larger bond order.

It is noted here that the $p_\sigma-p_\sigma$ overlap integral is moderately smaller than the $p_\pi-p_\pi$ one, unexpectedly. However, the $\sigma_p$ bond order is much larger than the $\pi_p$ bond order in both **S1** and **S2**,

unlike those of **M1** and **R1**. In these molecules, no group is present to destabilize the $\pi_p$ orbital energy, like the C−N bonds and negatively charged N atoms in **M1** and **R1**. Here, different factors are responsible for the larger occupation number of the $\sigma_p$ orbital than expected from the overlap integral. One plausible factor is nuclear−electron attraction like **M1** and **R1**. Another factor is the bonding participation of Si 3s orbital in the $\sigma_p$ orbital, which lowers the energy level of the $\sigma_p$ orbital through the bonding mixing, as shown in Scheme 3. On the other hand, the Si 3s orbital does not participate at all in the out-of-plane $\pi_p$ bonding orbital. In the in-plane $\pi_p$ orbital, the Si 3s orbitals participate in an antibonding manner, as shown in Scheme 3, which pushes up the in-plane $\pi_p$ orbital energy. In **M1** and **R1**, the 4s orbital of Cr contributes little to the $\sigma_d$ orbital because the Cr 4s orbital is at much higher energy than the Cr 3d orbital in Cr(II). Moreover, the difference between the $p_\sigma-p_\sigma$ overlap integral and the $p_\pi-p_\pi$ one in the Si−Si pair is much smaller than that between the $d_\sigma-d_\sigma$ overlap integral and the $d_\pi-d_\pi$ one in the Cr−Cr pair, as shown in Table 4. Therefore, despite the absence of the C−N bonds and the negatively charged N atom, the participation of Si 3s orbital and the nuclear−electron attraction are enough to overcome the consequence of the smaller $p_\sigma-p_\sigma$ overlap integral, leading to the larger occupation number of the $\sigma_p$ orbital than that of the $\pi_p$ orbital.

In conclusion, the interesting differences between M−M and Si−Si multiple bonds are summarized as follows: (1) The nondynamical correlation is much smaller in the Si−Si multiple bond than in the Cr(II)−Cr(II) multiple bond. (2) The $\sigma$-bonding interaction contributes much more to the Si−Si multiple bond than that to the M−M multiple bond.

## 4. Conclusion

We investigated open-lantern-type dinuclear Cr(II) complex, $[Cr(R^1NC(R^2)NR^3)_2]_2$ ($R^1$ = Et, $R^2$ = Me, and $R^3$ = $^t$Bu), with DFT, CASSCF, and MRMP2 methods. The DFT-calculated potential energy decreases as the Cr−Cr distance becomes shorter, and the equilibrium structure is not found in the range $R$(Cr−Cr) > 1.75 Å. In contrast to the DFT-calculated result, the CASSCF(8,8)-calculated potential energy decreases as the Cr−Cr distance becomes longer but does not present the minimum in the range $R$(Cr−Cr) < 2.05 Å. The MRMP2 calculation exhibits the minimum at $R$(Cr−Cr) = 1.851 Å, as shown in Figures 2 and 3. These results suggest that both nondynamical and dynamical correlations are considerably large in this complex. On the other hand, the nondynamical correlation is small in the Mo analogue; actually, the DFT, CASSCF, and MRMP2 methods present almost the same equilibrium Mo−Mo distance. The reason why the nondynamical correlation in the dinuclear Mo complex is smaller than in the dinuclear Cr complex is explained in terms of the overlap integral: actually the overlap integral of valence d orbitals in the Cr−Cr pair is much smaller than that of Mo−Mo pair. We wonder why the nondynamical correlation is very large although the Cr−Cr bond was experimentally discussed to be short in many dinuclear Cr complexes. To find answer to this issue, we wish to propose OSR (orbital shortness ratio) here to discuss the M−M multiple bond distance. The OSR value is 1.217 for real Cr complex **R1** and 0.854 for **Mo1**. Thus, we must understand that the Cr−Cr distance of 1.96 Å is long in **R1** but the Mo−Mo distance of 2.151 Å is short in **Mo1**. These understandings are consistent with the fact that the nondynamical correlation is much larger in the dinuclear Cr(II) complex than in the Mo(II) analogue.

The bond order of the real complex **R1** is evaluated to be 2.40, which is much smaller than the formal bond order of 4. That of the Mo analogue is evaluated to be 3.41, which is much larger than that of **R1**. These results agree with the fact that the nondynamical correlation is larger in the dinuclear Cr complex than in the Mo analogue.

Our calculations reveal that the overlap integral of valence $d_\pi$ orbital is much larger than that of $d_\sigma$ orbital in both Cr and Mo dinuclear complexes, and that of $p_\pi$ orbital is moderately larger than that of $p_\sigma$ orbital in $Si_2H_2$ and $Si_2H_4$. However, the occupation number of the $\sigma_d$ orbital is moderately larger than those of the $\pi_d$ orbitals in both the dinuclear Cr and Mo complex, and that of the $\sigma_p$ orbital is much larger than that of the $\pi_p$ orbital in both Si−Si double and triple bonds, contrary to the expectation from overlap integrals. In the Si−Si multiple bond, the Si 3s orbital contributes to the $\sigma_p$ orbital, leading to the lower orbital energy and the larger occupation number of the $\sigma_p$ orbital than expected from overlap integral. In the M−M multiple bond, the moderately larger occupation number of the $\sigma_d$ orbital arises from the smaller exchange repulsion between the $\sigma_d$ and the bridging ligand, the smaller Coulombic repulsion between the $\sigma_d$ and the negatively charged N atoms of ligands, and the larger nuclear−electron attraction between the electron density of the $\sigma_d$ and the M atoms than those of the $\pi_d$. Important differences between Cr−Cr and Si−Si multiple bonds are summarized as follows: (1) The nondynamical correlation is much larger in the Cr−Cr multiple bond than in the Si−Si multiple bond. (2) The $\sigma$-bonding interaction is much more important than the $\pi$-bonding interaction in the Si−Si multiple bond, while the $\sigma$-bonding interaction is moderately more important than the $\pi$-bonding interaction in the Cr−Cr multiple bond.

**Acknowledgment.** This research was supported in part by the Grant-in-Aids on Priority Area "Molecular Theory for Real Systems" (No. 461), NAREGI Project (Institute for Molecular Science; Okazaki, Japan), and Global COE Program "International Center for Integrated Research and Advanced Education in Materials Science" (No. B-09) of the Ministry of Education, Culture, Sports, Science and Technology (MEXT) of Japan and the Japan Society for the Promotion of Science. Some of theoretical calculations were performed at Institute for Molecular Science (Okazaki, Japan).

**Supporting Information Available:** Complete reference for Gaussian 03, GAMESS, and Molkel 5.2. Optimized geometries of **M1** (Table S1), **R1** (Table S2), **Mo1** (Table S3), **S1** and **S2** (Figure S1). Kohn−Sham orbitals of **S1** (Figure S2). Fully optimized geometries of **M1** (Figure S3). The PES of **M1** in the nonet spin state (Figure S4). The occupation numbers of **M1** (Figure S5), **R1** (Figure S6), and **Mo1** (Figure S7). PES of closed-lantern-type complex (Figure S8) and its important CASSCF configuration and coefficients (Table S4). Overlap integrals between two valence orbitals of M atom, $S^M_{d_a-d_a}(R)$, as a function of nuclear distance $R$ where M = N (Figure S9), M = Si (Figure S10), M = Cr (Figure S11), and M = Mo (Figure S12). This information is available free of charge via the Internet at http://pubs.acs.org.

## References and Notes

(1) Cotton, F. A.; Harris, C. B. *Inorg. Chem.* **1965**, *4*, 330.
(2) Cotton, F. A. *Inorg. Chem.* **1965**, *4*, 334.
(3) (a) Roos, B. O. *Adv. Chem. Phys.* **1987**, 399. (b) Andersson, K.; Malmqvist, P. A.; Roos, B. O.; Sadlej, A. J.; Wolinski, K. *J. Phys. Chem.* **1990**, *94*, 5483.
(4) (a) Hirao, K. *Chem. Phys. Lett.* **1992**, *190*, 374. (b) Hirao, K. *Chem. Phys. Lett.* **1992**, *196*, 397. (c) Nakano, H. *J. Chem. Phys.* **1993**, *99*, 7983.
(5) Goodgame, M. M.; Goddard, W. A., III. *J. Phys. Chem.* **1981**, *85*, 215.

(6) (a) Werner, H.-J.; Knowles, P. J. *J. Chem. Phys.* **1988**, *89*, 5803. (b) Andersson, K.; Roos, B. O.; Malmqvist, P.-A.; Widmark, P.-O. *Chem. Phys. Lett.* **1994**, *230*, 391. (c) Roos, B. O.; Andersson, K. *Chem. Phys. Lett.* **1995**, *245*, 215. (d) Edgecombe, K. E.; Becke, A. D. *Chem. Phys. Lett.* **1995**, *244*, 427. (e) Thomas, E. J.; Murray, J. S.; O'Connor, C. J.; Politzer, P. *J. Mol. Struct. (Theochem)* **1999**, *487*, 177. (f) Barden, C. J.; Rienstra-Kiracofe, J. C.; Schaefer, H. F. *J. Chem. Phys.* **2000**, *113*, 690. (g) Angell, C.; Cimiraglia, R.; Malrieu, J.-P. *J. Chem. Phys.* **2002**, *117*, 9138. (h) Celani, P.; Stoll, H.; Werner, H.-J.; Knowles, P. *J. Mol. Phys.* **2004**, *102*, 2369. (i) Roos, B. O.; Borin, A. C.; Gagliardi, L. *Angew. Chem., Int. Ed. Engl.* **2007**, *46*, 1469.

(7) Nguyen, T.; Sutton, A. D.; Brynda, M.; Fettinger, J. C.; Long, G. J.; Power, P. P. *Science* **2005**, *310*, 844.

(8) Landis, C. R.; Weinhold, F. *J. Am. Chem. Soc.* **2006**, *128*, 7335.

(9) Merino, G.; Donald, K. J.; D'Acchioli, J. S.; Hoffmann, R. *J. Am. Chem. Soc.* **2007**, *129*, 15295.

(10) Brynda, M.; Gagliardi, L.; Widmark, P.-O.; Power, P. P.; Roos, B. O. *Angew. Chem., Int. Ed. Engl.* **2006**, *45*, 3804.

(11) Hsu, C.-W.; Yu, K. J.-S.; Yen, C.-H.; Lee, G.-H.; Wang, Y.; Tsai, Y.-C. *Angew. Chem., Int. Ed. Engl.* **2008**, *47*, 9933.

(12) (a) Cotton, F. A.; Extine, M.; Rice, G. W. *Inorg. Chem.* **1978**, *17*, 176. (b) Cotton, F. A.; Murillo, C. A.; Walton, R. A. *Multiple Bond between Metal Atoms*, 3rd. ed.; Springer, Berlin, 2005.

(13) (a) Mashima, K.; Tanaka, M.; Tani, K.; Nakamura, A.; Takeda, S.; Mori, W.; Yamaguchi, K. *J. Am. Chem. Soc.* **1997**, *119*, 4307. (b) Nishino, M.; Yamanaka, S.; Yoshioka, Y.; Yamaguchi, K. *J. Phys. Chem. A* **1997**, *101*, 705. (c) Nishino, M.; Yoshioka, Y.; Yamaguchi, K.; Mashima, K.; Tani, K.; Nakamura, A. *Bull. Chem. Soc. Jpn.* **1998**, *71*, 99.

(14) de Mello, P. C.; Edwards, W. D.; Zerner, M. C. *J. Am. Chem. Soc.* **1982**, *104*, 1440.

(15) (a) Hao, S.; Gambarotta, S.; Bensimon, C. *J. Am. Chem. Soc.* **1992**, *114*, 3556. (b) Edema, J. J. H.; Gambarotta, S.; Bolhuis, F. V.; Spek, A. L. *J. Am. Chem. Soc.* **1989**, *111*, 2142. (c) Edema, J. J. H.; Gambarotta, S.; Meetsma, A.; Bolhuis, F. V.; Spek, A. L.; Smeets, W. J. J. *Inorg. Chem.* **1990**, *29*, 2147. (d) Hao, S.; Song, J.-I.; Berno, P.; Gambarotta, S. *Organometallics* **1994**, *13*, 1326. (e) Edema, J. J. H.; Gambarotta, S.; van der Sluis, P.; Smeets, W. J. J.; Spec, A. L. *Inorg. Chem.* **1989**, *28*, 3782. (f) Hao, S.; Gambarotta, S.; Bensimon, C.; Edema, J. J. H. *Inorg. Chim. Acta* **1993**, *213*, 65.

(16) Li, S.; King, R. B.; Schaefer, H. F., III. *J. Phys. Chem. A.* **2004**, *108*, 6879.

(17) Becke, F.; Wiegeleben, P.; Ruffer, T.; Wagner, C.; Boese, R.; Blaser, D.; Steinborn, D. *Organometallics* **1998**, *17*, 475.

(18) Losada, J.; Alvarez, S.; Novoa, J. J.; Mota, F.; Hoffmann, R.; Silvestre, J. *J. Am. Chem. Soc.* **1990**, *112*, 8998.

(19) Brauer, D. J.; Krueger, C. *Inorg. Chem.* **1976**, *15*, 2511.

(20) Ziegler, T. *J. Am. Chem. Soc.* **1985**, *107*, 4453.

(21) (a) Mitschler, A.; Rees, B.; Wiest, R.; Benard, M. *J. Am. Chem. Soc.* **1982**, *104*, 7501. (b) Benard, M. *J. Am. Chem. Soc.* **1978**, *100*, 2354.

(22) Manning, M. C.; Trogler, W. C. *J. Am. Chem. Soc.* **1983**, *105*, 5311.

(23) Lichtenberger, D. L.; Lynn, M. A.; Chisholm, M. H. *J. Am. Chem. Soc.* **1999**, *121*, 12167.

(24) El-Kadri, O. M.; Heeg, M. J.; Winter, C. H. *Inorg. Chem.* **2006**, *45*, 5278.

(25) Chang, H. C.; Li, J. T.; Wang, C. C.; Lin, T. W.; Lee, H. C.; Lee, G. H.; Peng, S. M. *Eur. J. Inorg. Chem.* **1999**, *8*, 1243.

(26) Morse, P. M.; Spencer, M. D.; Wilson, S. R.; Girolami, G. S. *Organometallics* **1994**, *13*, 1646.

(27) Garner, C. D.; Senior, R. G.; King, T. J. *J. Am. Chem. Soc.* **1976**, *98*, 3526.

(28) Sadique, A. R.; Heeg, M. J.; Winter, C. H. *J. Am. Chem. Soc.* **2003**, *125*, 7774.

(29) (a) Becke, A. D. *J. Chem. Phys.* **1993**, *98*, 5648. (b) Lee, C.; Yang, W.; Parr, R. G. *Phys. Rev. B* **1988**, *37*, 785.

(30) Saito, K.; Nakao, Y.; Sato, H.; Sakaki, S. *J. Phys. Chem. A* **2006**, *110*, 9710.

(31) Blaudeau, J.-P.; Ross, R. B.; Pitzer, R. M. *J. Phys. Chem.* **1994**, *98*, 7123.

(32) Dapprich, S.; Komaromi, I.; Byun, K. S.; Morokuma, K.; Frisch, M. J. *J. Mol. Struct. (Theochem)* **1999**, *461*, 1.

(33) (a) Bergner, A.; Dolg, M.; Kuechle, W.; Stoll, H.; Preuss, H. *Mol. Phys.* **1993**, *80*, 1431. (b) Dolg, M.; Wedig, U.; Stoll, H.; Preuss, H. *J. Phys. Chem.* **1987**, *86*, 866.

(34) Sekiguchi, A.; Kinjo, R.; Ichinohe, M. *Science* **2004**, *305*, 1755.

(35) Frisch, M. J.; Pople J. A.; et al. *Gaussian 03,* revision C.02; Gaussian, Inc.: Wallingford, CT, 2004.

(36) Schmidt, M. W.; et al. *J. Comput. Chem.* **1993**, *14*, 1347.

(37) Molekel ver.5.2, Swiss National Supercomputing Centre.

(38) Fully optimized geometry of **M1** takes $C_s$ symmetry with reflection mirror being on the C−Cr−Cr−C plane (Supporting Information Figure S3). This geometry is considerably different from that of real complex. We carried out preliminary examination with the geometry of **M1** shown in Figure 1, because the imaginary frequency is very small, and moreover PESs of **M1** are essentially the same as those of **R1**.

(39) Cotton, F. A.; Hillard, E. A.; Murillo, C. A. *J. Am. Chem. Soc.* **2003**, *123*, 2026.

(40) Li, Q.-s.; Zhang, X.; Xie, Y.; King, R. B.; Schaefer, H. F. *J. Am. Chem. Soc.* **2007**, *129*, 3433.

(41) In CASSCF calculation, the orbital energy is not defined. The large occupation number corresponds, in general, to the low energy of the canonical orbital which is the main contributor of the natural orbital.

(42) (a) Pou-Amerigo, R.; Merchan, M.; Nebot-Gil, I.; Widmark, P.-O.; Roos, B. O. *Theor. Chim. Acta.* **1995**, *92*, 149. (b) Widmark, P.-O.; B.; Joakim, Persson; Roos, B. O. *Theor. Chim. Acta* **1991**, *79*, 419.

(43) Huzinaga, S. *Gaussian basis sets for molecular calculations*; Elsevier Science Publishing Company, Inc.: New York, 1984.

(44) Wang, Y.; Xie, Y.; Wei, P.; King, R. B.; Schaefer, H. F.; Schleyer, P. v. R.; Robinson, G. H. *Science* **2008**, *321*, 1069.

(45) Frenking, G.; Fröhlich, N. *Chem. Rev.* **2000**, *100*, 717.

JP809597M